Electronic Supplementary Information

Self-assembled block copolymer micelles with silver-carbon nanotube hybrid fillers for high performance thermal conduction†

Jae Ryung Choi,‡[a] Seunggun Yu,‡[ab] Haejong Jung,[a] Sun Kak Hwang,[a] Richard Hahnkee Kim,[a] Giyoung Song,[a] Sung Hwan Cho,[a] Insung Bae,[a] Soon Man Hong,[b] Chong Min Koo*[b] and Cheolmin Park*[a]

[a] *Department of Materials Science and Engineering, Yonsei University, Seoul, 120-749, Republic of Korea. E-mail: cmpark@yonsei.ac.kr*

[b] *Center for Materials Architecturing, Korea Institute of Science and Technology, Seoul, 136-791, Republic of Korea*

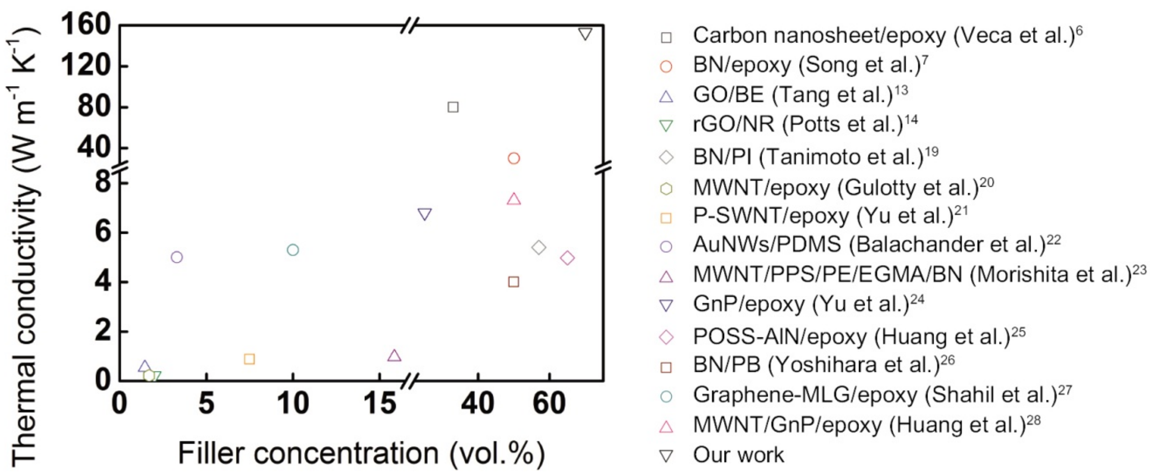

Fig. S1 Representative thermal conductivity studies of highly filled polymer composites.

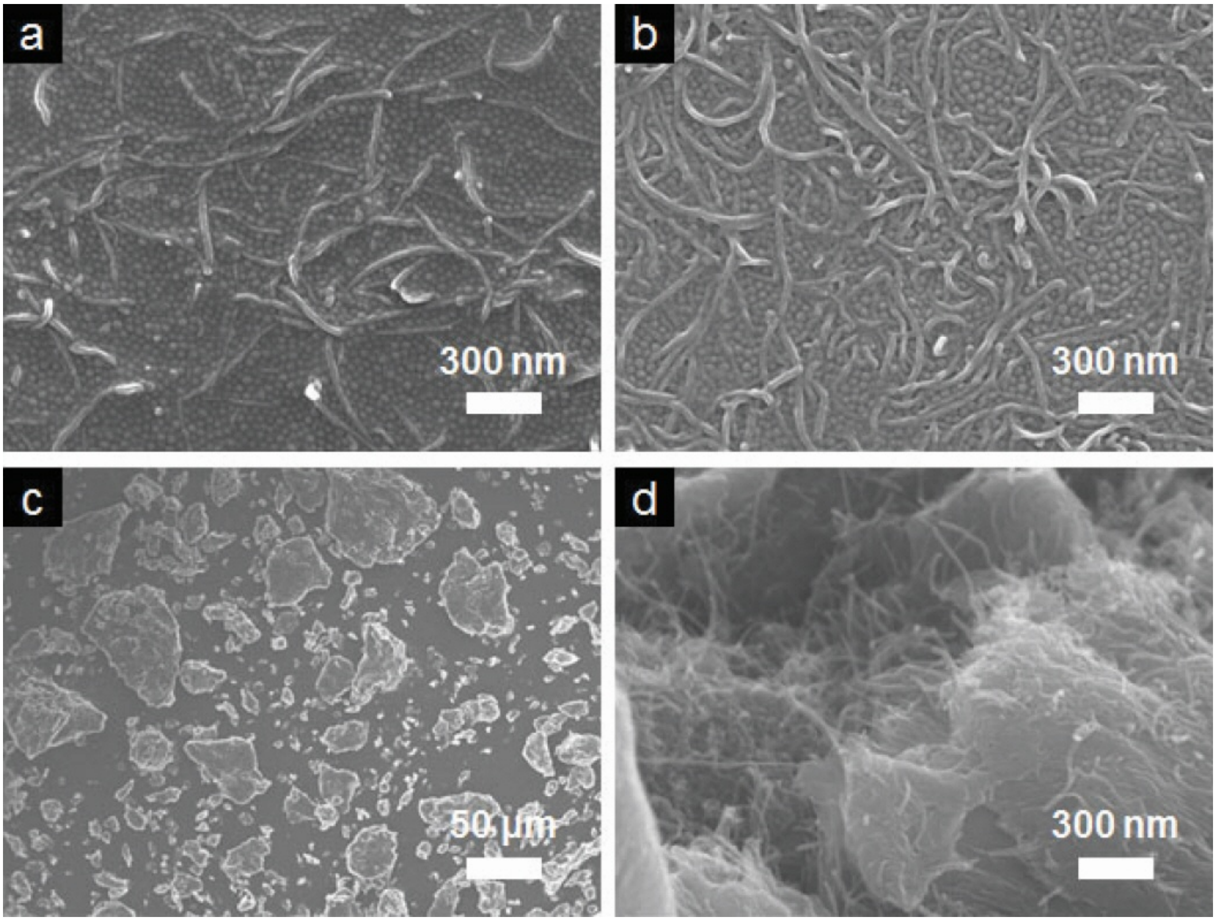

Fig. S2 (a and b) SEM images of MWNTs/PS-*b*-P4VP composite mat prepared by vacuum filtration from an MWNT and PS-*b*-P4VP solution in toluene. The MWNTs were uniformly dispersed with self-assembled PS-*b*-P4VP micelles. (c and d) SEM images of fine MWNTs/PS-*b*-P4VP composite powders with sizes of 10–50 μm a mechanical milling process. A magnified image of (d) shows numerous MWNTs reinforced and networked in the block copolymer.

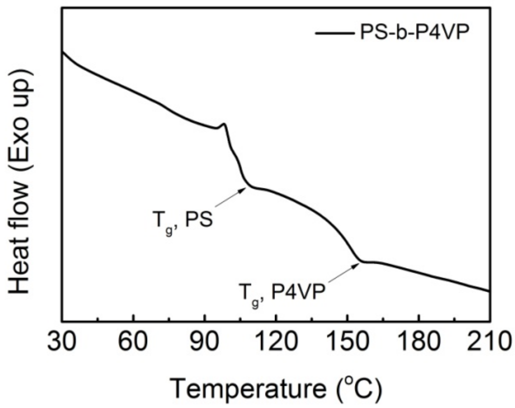

Fig. S3 DSC trace of pristine PS-*b*-P4VP upon heating from 30 to 210 °C with a heating rate of 2 °C/min. The glass transition temperatures of PS and P4VP blocks were 98 and 156 °C, respectively.

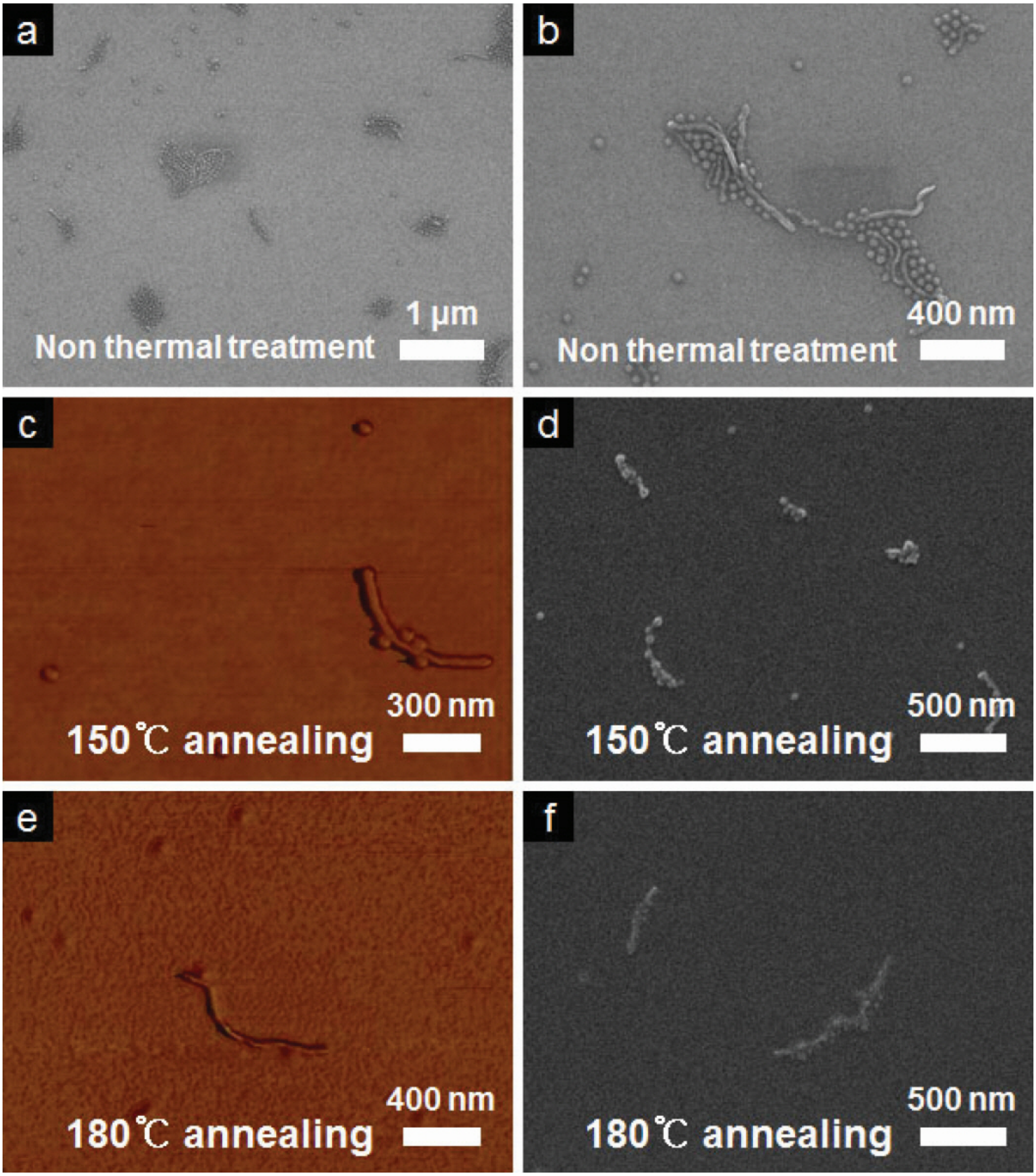

Fig. S4 (a, c, e) Phase contrast TM-AFM images and (b, d, f) SEM images of MWNTs decorated with PS-*b*-P4VP micelles at different annealing temperatures. Micelles individually isolated at room temperature were fused with each other to cover the surface of the nanotube upon heat treatment.

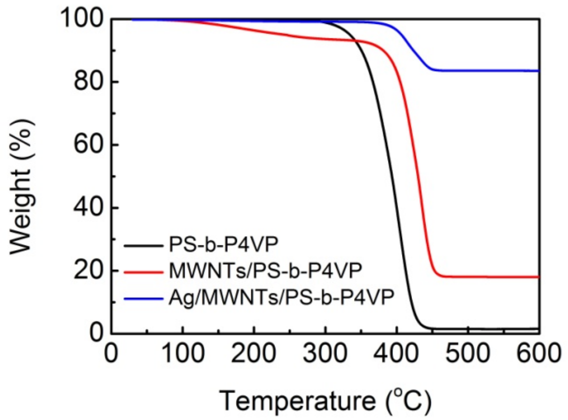

Fig. S5 TGA curves of a pristine PS-*b*-P4VP sample, a MWNTs/PS-*b*-P4VP composite and an Ag/MWNTs/PS-*b*-P4VP hybrid composite with 70 vol.% Ag.

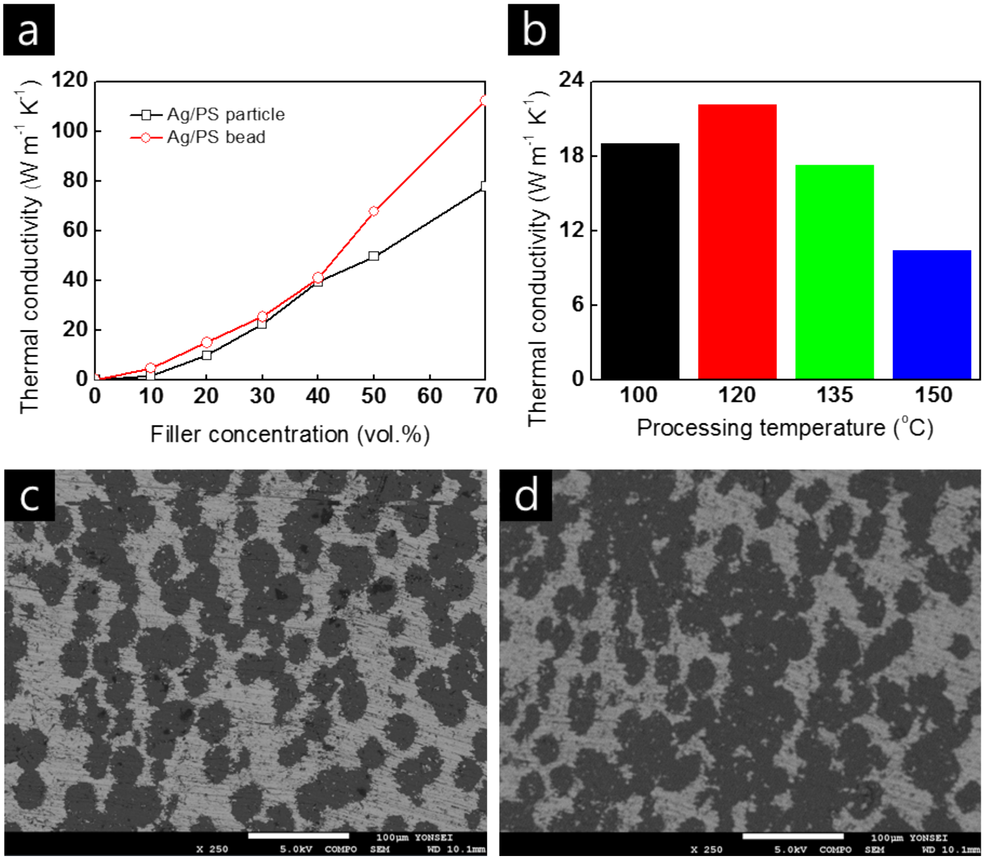

Fig. S6 (a) Thermal conductivity Ag/PS particle and Ag/PS colloid composites processed at 120 °C. (b) Thermal conductivity Ag/PS colloid composites (30 vol.%) with various processing temperature. (c and d) SEM images of the Ag/PS colloid composites processed at 120 °C and 150 °C, respectively. Ag and PS beads appear bright and dark in the micrographs, respectively. The colloids were readily molten during compression at 150 °C and thus the structural matrix did not exist any more. As expected, the composite shows its thermal conductivity approximately half of that of a composite processed at 120 °C as shown in (b). SEM analysis revealed that more continuous pathways of Ag particles (bright parts) were formed in the sample prepared at 120 °C than one at 150 °C.

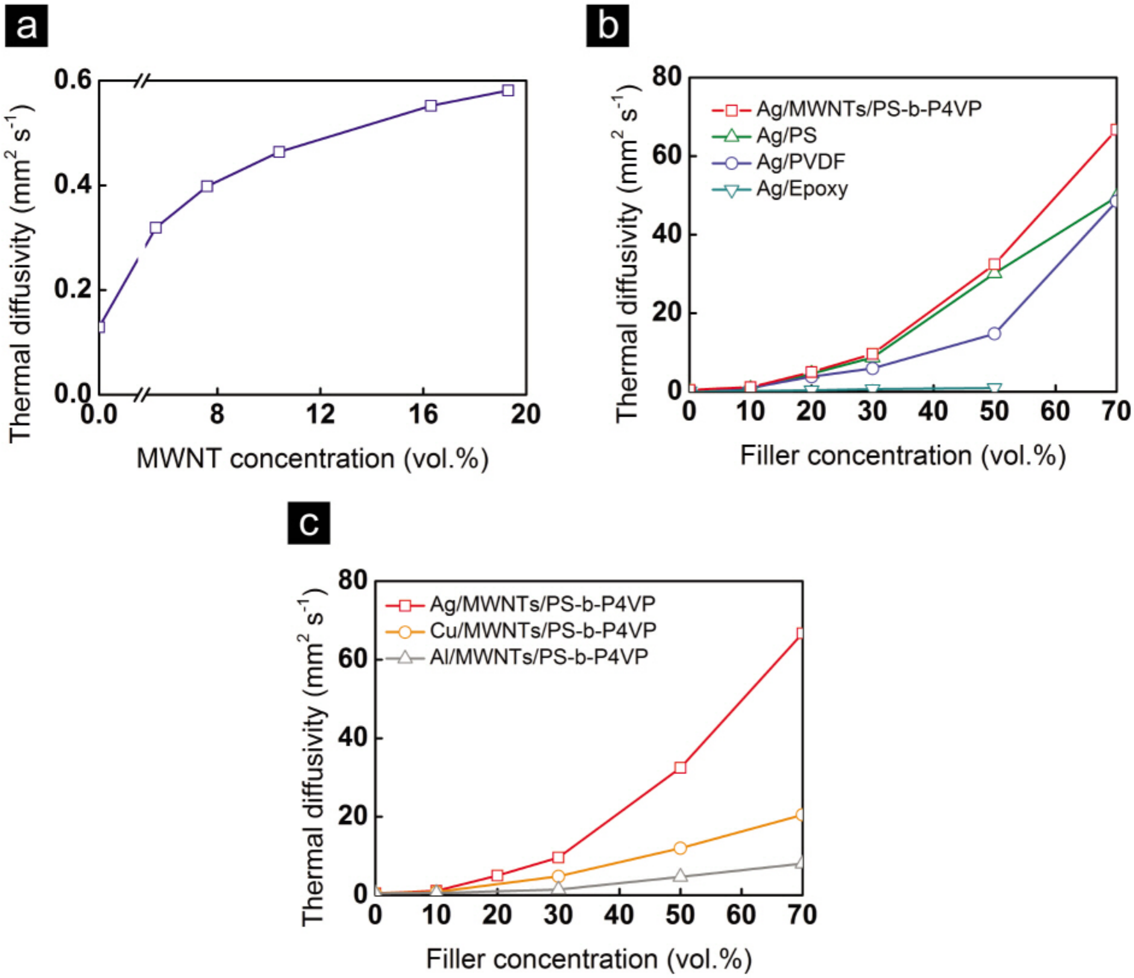

Fig. S7 Thermal diffusivities of the composites. (a) MWNTs/PS-*b*-P4VP composites with various loadings of MWNTs. (b) Ag/MWNTs/PS-*b*-P4VP composites with 2-μm Ag particles as a function of the concentration of Ag particles. Ag/PS, Ag/PVDF and Ag/epoxy composites were also examined for comparison. (c) Metal/MWNTs/PS-*b*-P4VP hybrid composites as a function of the metal concentration with various metal particles of Ag, Al and Cu.

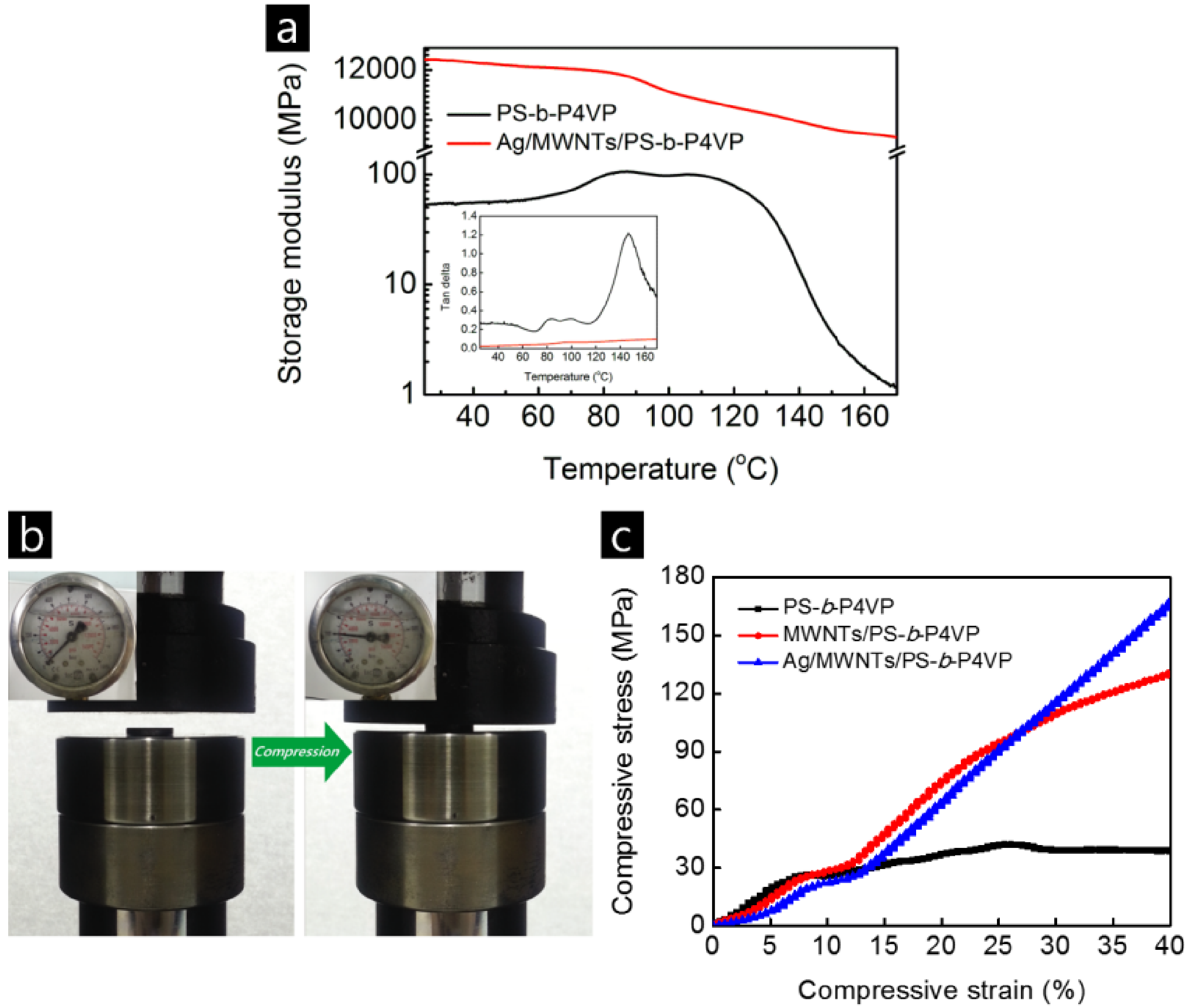

Fig. S8 (a) Storage modulus curves of PS-*b*-P4VP and Ag/MWNTs/PS-*b*-P4VP composites. The inset shows tanδ curves of the composites. (b) Photographs of the Ag/MWNTs/PS-*b*-P4VP composites before and after pressure induced. The measured pressure gauge is highlighted on the top of each image. For instance, under the pressure of 200 bar, our hybrid composite was rarely fractured. (c) Compression stress-strain curves of PS-b-P4VP, MWNTs/PS-b-P4VP and Ag/MWNTs/PS-b-P4VP composites.

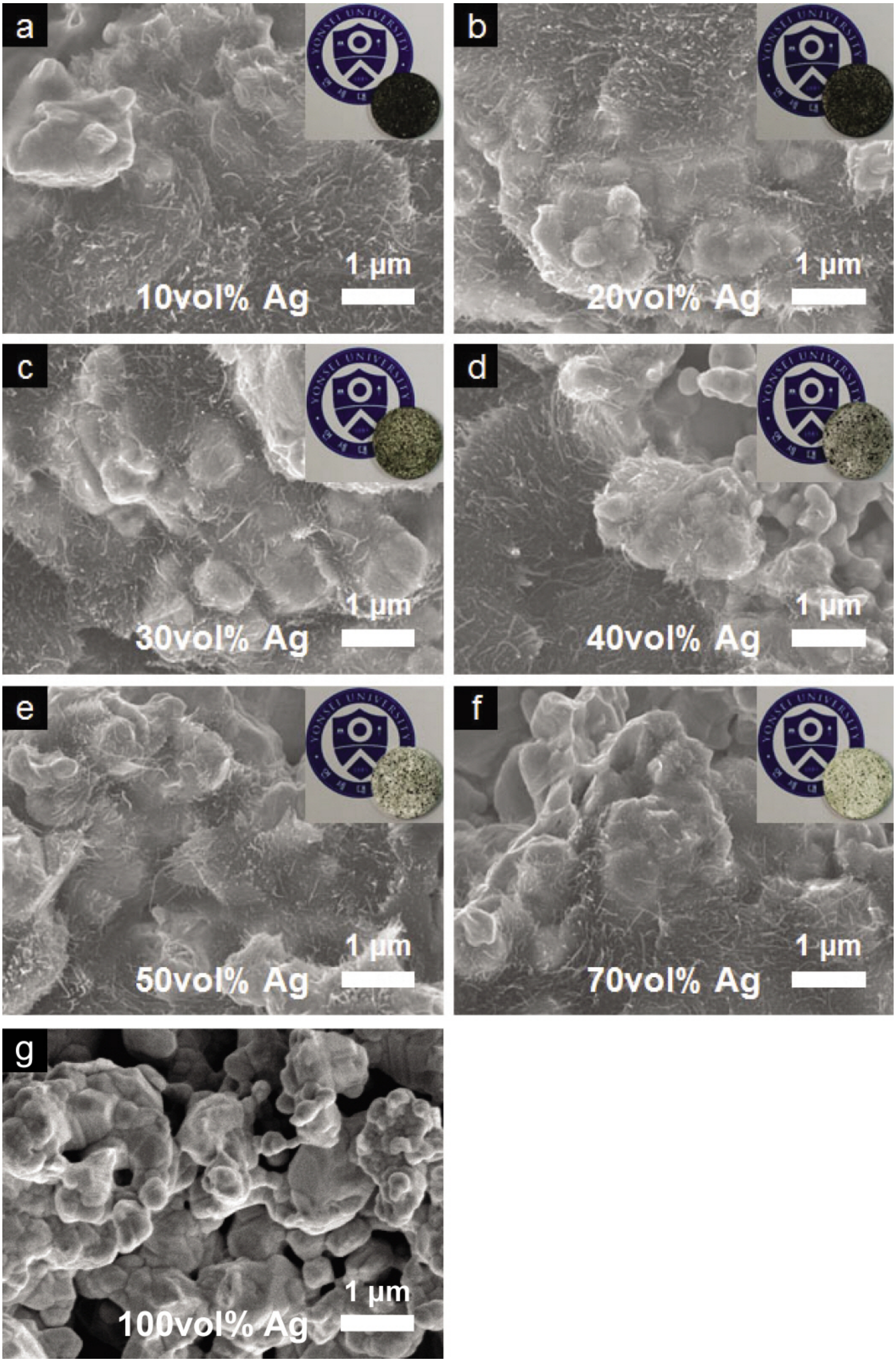

Fig. S9 SEM images of the fractured surfaces of Ag/MWNTs/PS-*b*-P4VP hybrid composites as a function of filler concentration. Photographs of the hybrid composites were highlighted on the top of each image.

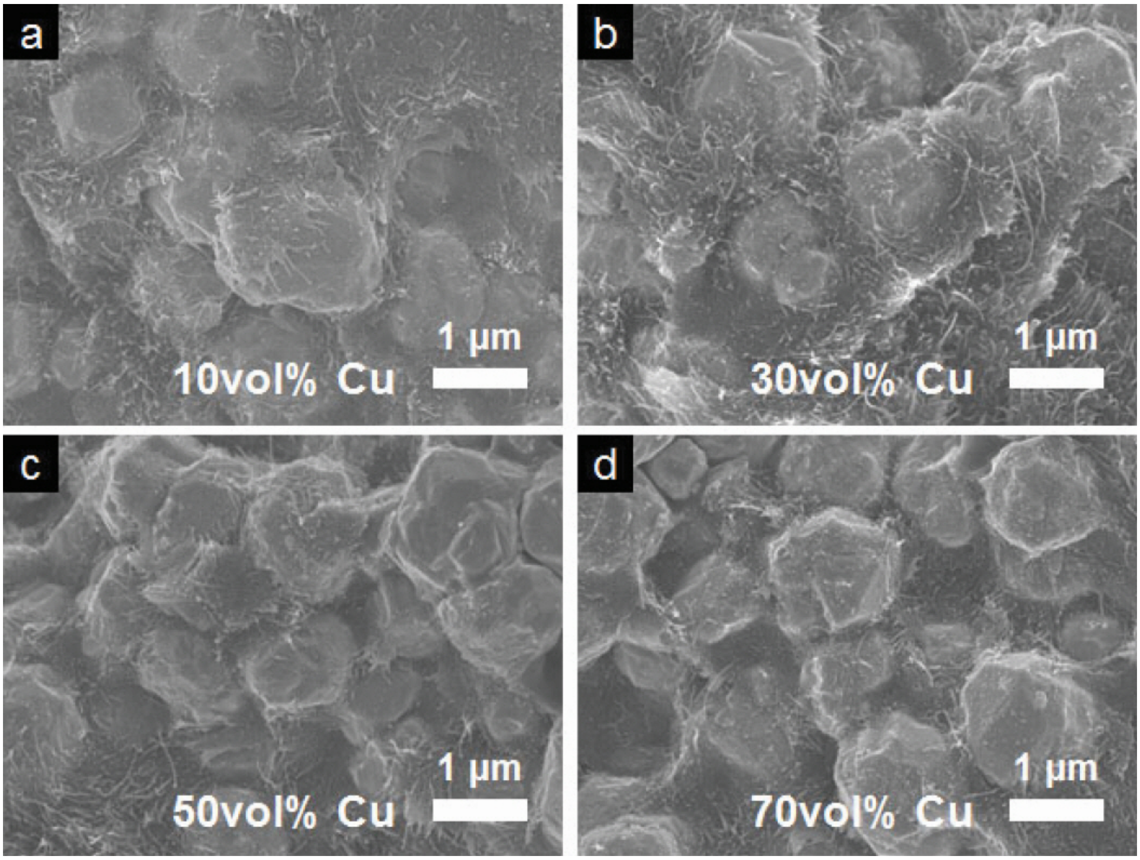

Fig. S10 SEM images of the fractured surfaces of Cu/MWNTs/PS-*b*-P4VP hybrid composites as a function of filler concentration.

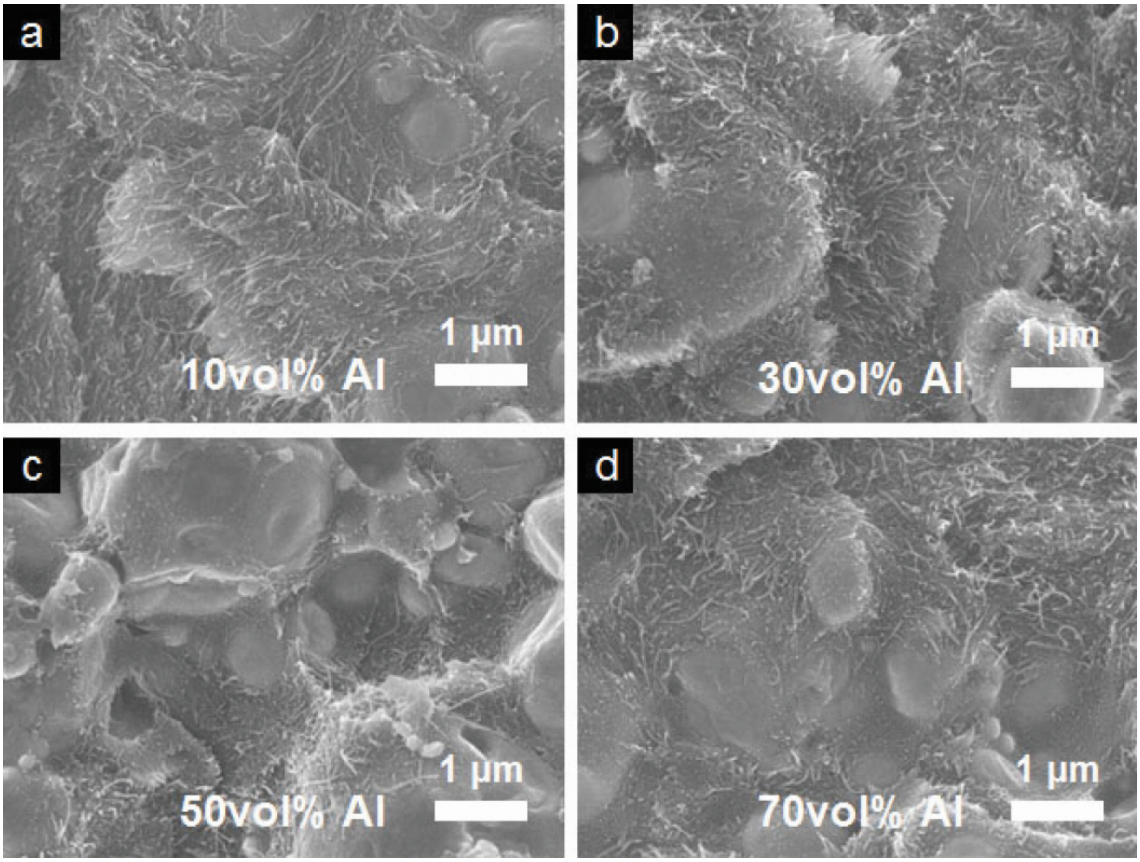

Fig. S11 SEM images of the fractured surfaces of Al/MWNTs/PS-*b*-P4VP hybrid composites as a function of filler concentration.

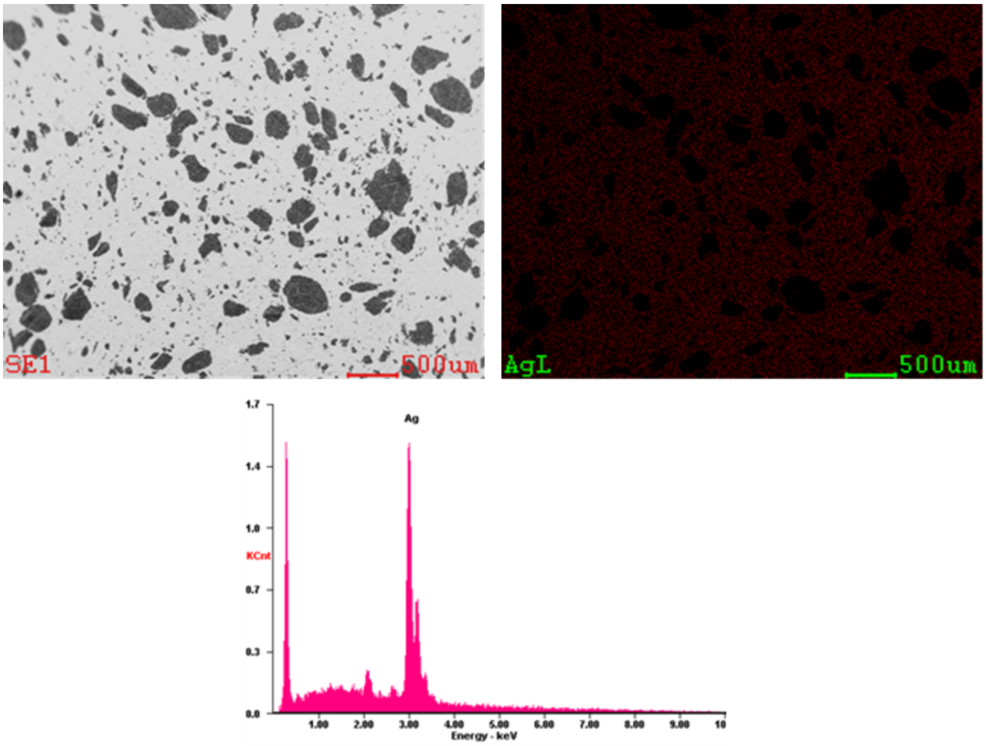

Fig. S12 SEM image and EDS spectrum of the polished surface of an Ag/MWNTs/PS-b-P4VP hybrid composite.

Table S1 The characteristics of MWNTs/PS-*b*-P4VP composites, metal/MWNTs/PS-*b*-P4VP hybrid composites, Ag/PS composites and Ag/PVDF composites including composition, density and specific heat data.

Sample	Content (wt.%)			Content (vol.%)			Density (g cm^{-3})	Specific heat (J g^{-1} K^{-1})
	Metal	MWNTs	PS-*b*-P4VP	Metal	MWNTs	PS-*b*-P4VP		
MWNTs/PS-*b*-P4VP	-	9.1	90.9	-	5.6	94.4	1.20	1.04
	-	12.5	87.5	-	7.6	92.4	1.18	1.05
	-	16.7	83.3	-	10.4	89.6	1.13	1.10
	-	25.0	75.0	-	16.3	83.7	1.08	1.13
	-	33.3	66.7	-	19.3	80.7	1.09	1.12
Ag/MWNTs/PS-*b*-P4VP	50.2	9.4	40.4	10.0	9.4	80.6	2.00	0.71
	69.4	5.8	24.8	20.0	8.3	71.7	2.99	0.53
	87.4	4.3	18.3	30.0	7.3	62.7	3.70	0.47
	90.0	1.9	8.1	50.0	5.2	44.8	5.02	0.35
	95.5	0.8	3.7	70.0	3.1	26.9	7.80	0.32
Ag/PS	-	-	100.0	-	-	100.0	1.04	1.40
	52.8	-	47.2	10.0	-	90.0	2.02	0.83
	71.6	-	28.4	20.0	-	80.0	3.02	0.65
	81.2	-	18.8	30.0	-	70.0	3.89	0.51
	91.0	-	9.0	50.0	-	50.0	5.44	0.39
	95.9	-	4.1	70.0	-	30.0	6.93	0.35
Ag/PVDF	-	-	100.0	-	-	100.0	1.49	1.37
	43.9	-	56.1	10.0	-	90.0	2.23	0.87
	63.8	-	36.2	20.0	-	80.0	3.26	0.67
	75.1	-	24.9	30.0	-	70.0	4.15	0.56
	87.6	-	12.4	50.0	-	50.0	5.22	0.41
	94.3	-	5.7	70.0	-	30.0	7.42	0.32
Cu/MWNTs/PS-*b*-P4VP	46.2	10.2	43.6	10.0	9.4	80.6	1.91	1.08
	76.8	4.4	18.8	30.0	7.3	62.7	3.44	1.02
	88.5	2.3	9.4	50.0	5.2	44.8	4.62	1.06
	94.7	1.0	4.3	70.0	3.1	26.9	5.44	1.10
Al/MWNTs/PS-*b*-P4VP	20.6	15.0	64.4	10.0	9.4	80.6	1.19	0.90
	49.9	9.5	40.6	30.0	7.3	62.7	1.49	0.53
	70.0	5.7	24.3	50.0	5.2	44.8	1.80	0.47
	84.5	2.9	12.6	70.0	3.1	26.9	1.92	0.44

5